New Journal of Physics
The open–access journal for physics

Photonic crystal and photonic wire nano-photonics based on silicon-on-insulator

Richard De La Rue[1], Harold Chong[1], Marco Gnan[1], Nigel Johnson[1], Iraklis Ntakis[1], Pierre Pottier[1], Marc Sorel[1], Ahmad Md Zain[1], Hua Zhang[1], Edilson Camargo[2], Chongjun Jin[3], Mario Armenise[4] and Caterina Ciminelli[4]

[1] Optoelectronics Research Group, Department of Electronics and Electrical Engineering, University of Glasgow, Glasgow G12 8QQ, UK
[2] Institute of Aeronautics and Space (IAE/CTA), Praça Marechal Eduardo Gomes, 50, São José dos Campos - São Paulo, 12228-904, Brazil
[3] Department of Physics and Department of Chemistry, University of Toronto, Toronto, Canada
[4] Laboratorio di Ottoelettronica, Dipartimento di Elettrotecnica ed Elettronica, Politecnico di Bari, Via Orabona 4, 70125, Bari, Italy
E-mail: r.delarue@elec.gla.ac.uk

New Journal of Physics **8** (2006) 256
Received 4 August 2006
Published 26 October 2006
Online at http://www.njp.org/
doi:10.1088/1367-2630/8/10/256

Abstract. Silicon-on-insulator (SOI) is a strong candidate for application in future planar waveguide integration technology, whether or not luminescence is extracted from the silicon. We review recent research on photonic devices based on silicon-on-insulator. These devices exploit either photonic crystal or photonic wire concepts—or combinations of both. Aspects of the technologies used that are particularly critical for successful implementation of SOI-based photonics are addressed.

PII: S1367-2630(06)30128-0

Contents

1. Introduction 2
2. Silicon wafers as substrates for template applications 3
3. Photonic wire Bragg-grating structures 3
4. Photonic crystal channel waveguide devices 5
5. Photonic wire Mach–Zehnder devices 10
6. Finite area photonic crystal elements 12
7. Concluding remarks 14
Acknowledgments 14
References 14

1. Introduction

Single-crystal silicon continues to play a dominant role in electronics—and the silicon chip is nearly universal in a wide range of applications. The possibilities for using single-crystal silicon in optoelectronics and photonics have also been recognized for some time. Silicon provides the basis for excellent photo-detector devices that cover the entire visible spectrum and a useful, but limited, part of the infrared spectrum. Integration of photo-detection with various versions of silicon electronics is commercially viable at the level of the individual photo-receiver and at the level of the many pixel camera chip. Guided-wave optics in silicon has also been an important research topic for more than thirty years—and the recognition that silicon-on-insulator (SOI) technology could be exploited for planar waveguide-based photonics/optoelectronics, in particular for integrated optics, has launched a substantial level of commercially oriented research and development activity.

Efficient electroluminescent generation of light at a chosen wavelength or over a range of wavelengths—and with a chosen degree of coherence—is of central importance in optoelectronics and photonics. To date it has been mainly the direct band-gap III–V semiconductors—such as gallium-arsenide (GaAs), indium-phosphide (InP) and gallium-nitride (GaN)—that have provided the important base materials for electroluminescent devices. In contrast, silicon is not only an indirect band-gap semiconductor but it has also not readily adapted to the kind of doping approach that has been remarkably successful in the case of another III–V semiconductor used in electroluminescent devices, gallium phosphide (GaP). GaP, although is an indirect band-gap semiconductor, also can be doped with elements such as oxygen and nitrogen in a sufficiently controlled manner that fairly efficient electroluminescence can be produced in selected parts of the visible spectrum—via a high density of states induced in its electronic bandgap by the dopant atoms. GaP continues to be used extensively in light-emitting diodes (LEDs)—but not, despite its role in their early development, in semiconductor lasers.

This paper will not attempt to address the ongoing question of how silicon can be coaxed into becoming a viable electroluminescent medium, but instead will explore some of the interesting possibilities for photonic device technology that result from applying photonic crystal and photonic wire concepts on a base of silicon technology. The phrase ‘silicon technology’ will for our purposes embrace a range of techniques that include, for example, both the deep ultraviolet (DUV) lithography that is in routine use in very large scale integrated (VLSI) circuit

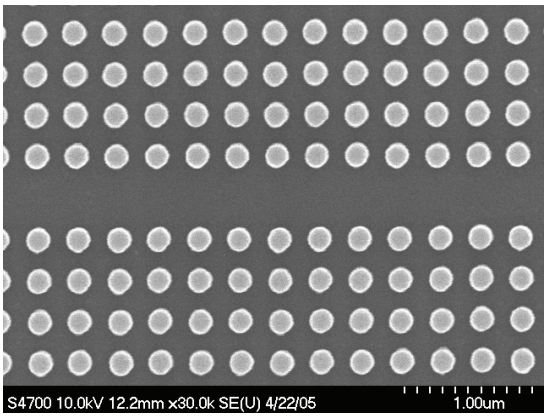

Figure 1. Scanning electron micrograph of template of circular pillars (with a defect inducing gap) produced by exposing and developing HSQ resist on a silicon substrate (see [1]).

production and the electron-beam lithography (EBL) that may only be used, for example, in pattern generation of masks for VLSI production. But EBL, in direct-write mode, has become the pattern generation tool of choice for many of the photonic crystal and photonic wire device structures of current research interest.

2. Silicon wafers as substrates for template applications

One example of a situation in which planar silicon technology has an impact on photonic crystal fabrication is the use of templates patterned in a suitable resist material to provide direct control on the orientation of the growth of opal-type three dimensional (3D) PhC structures [1]. Nominally (100)-oriented face-centred cubic (fcc) opal formed from polymer spheres has been grown by the 'vertical capillary growth' technique, using as templates, square arrays of pillars defined by EBL in HSQ negative resist on a silicon substrate, as shown in figure 1 and figure 2. While the use of substrates of single-crystal silicon for this purpose is not an unavoidable requirement, the properties of flatness and a significant amount of electrical conductivity provided by commercial silicon wafers are relevant to the growth of high-quality opal. Studies have also shown that, in the opal grown, a significant degree of tetragonal distortion from the purely cubic situation is possible. Although this study was based on the use of EBL, where a field size of approx. 0.25 mm^2 is typical, the template method is intrinsically applicable over much larger areas, up to whole silicon wafer scale, while taking account of levels of field stitching-error that are practically feasible with EBL. Opal type structures—and inverse-opal structures in a variety of material systems—could possibly be produced as 'single-domain' photonic crystals with the same level of perfection over a full wafer.

3. Photonic wire Bragg-grating structures

In the example cited above, sections of silicon wafer were used as substrates for EBL pattern-generation of templates for self-organized photonic crystal growth. Moving from simple silicon wafers to wafers of silicon-on-insulator (SOI) implies a relatively small modification

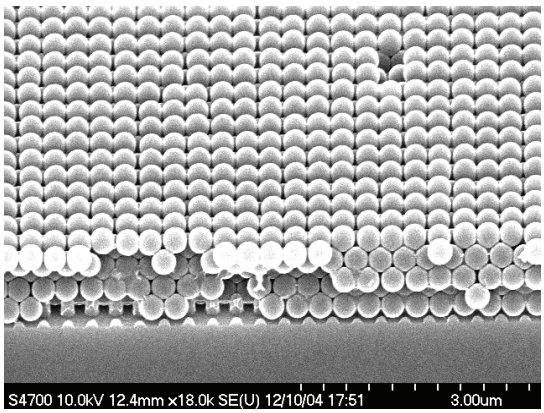

Figure 2. Scanning electron micrograph of cleaved (100)-oriented synthetic opal. (see [1]).

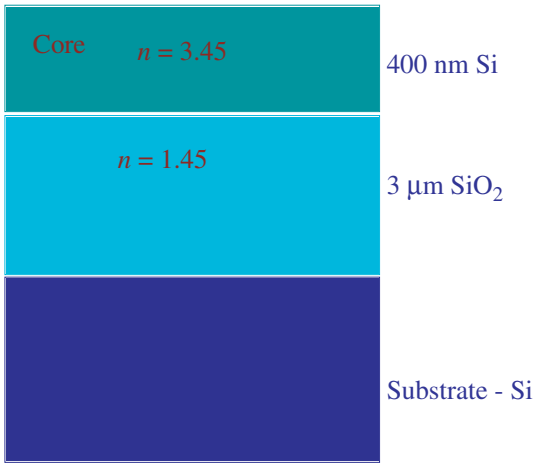

Figure 3. Schematic of SOI wafer section.

to processing conditions, and retains the useful property that there is sufficient electrical conductivity for charge dissipation during the writing process. But SOI is also a natural material system to use for planar optics and, in particular, guided-wave planar optics. Propagation losses can be acceptably small for infrared wavelengths such as 1.3 or 1.55 μm in pure silicon. Commercial-scale integrated optics based on waveguides in SOI has become a real possibility, although the matter of light generation and detection has to be addressed in a hybrid manner, using the III–V semiconductor-based devices that remain the norm for fibre-optical telecomm applications.

As shown in the schematic of figure 3, a typical SOI wafer for planar guided-wave optics purposes will have a silica lower-cladding thickness of about 3 μm, and a silicon core thickness of a few hundred nanometres. For the vertically asymmetric case in which there is 'air' above a silicon core that is supported by a silica lower-cladding layer, a core thickness of around 240 nm is indicated for maximization of the guided-mode effective refractive index while avoiding multimode propagation, at operating wavelengths around 1550 nm. Figure 4 shows a micrograph of a circa 500 nm wide photonic-wire rib waveguide etched into a section of SOI wafer after chemical vapour deposition (CVD) of an additional silica layer to form an upper cladding layer.

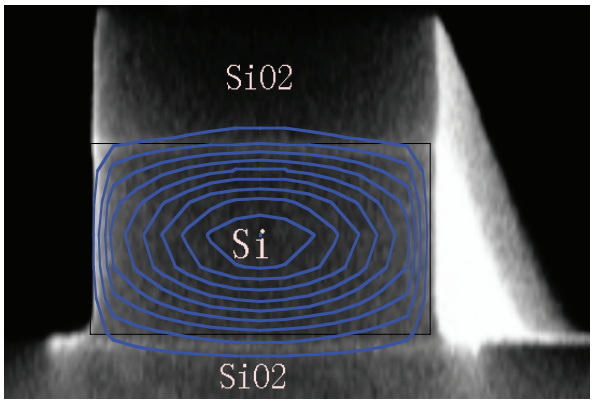

Figure 4. Scanning electron micrograph of silicon photonic wire waveguide with top cladding layer of deposited SOI. The superimposed contours indicate the fundamental mode distribution.

It may be useful, when forming planar waveguide-based photonic crystal or photonic wire structures, to start with a core waveguide thickness that is substantially larger than the value of 240 nm quoted above, and then reduce the thickness by a combination of processes such as thermal oxidation and wet-etching. SOI waveguides may also be processed to have a symmetric (or near-symmetric) vertical refractive-index distribution. Such a distribution may be obtained either by embedding the silicon waveguide core in silica, both above and below, or by removing the silica completely to form a suspended membrane, surrounded by air. For membranes, the issue of specifying a structure that is mechanically feasible cannot be avoided, although we are tempted to suggest that mechanical support could be provided by a low-density foam-type material, if the associated optical scattering level could be made sufficiently small. In designing and fabricating photonic crystal or photonic wire devices based on SOI, it is also necessary to consider the effective refractive indices produced locally in the structure.

The micrographs of figures 5(a) and (b) both show photonic wire Bragg grating structures realized in SOI, after pattern transfer into the silicon waveguide core using dry-etch processing. The use of hydrogen silsesquioxane (HSQ) resist (figure 5(b)), in place of a combination of ZEP[5] or PMMA (poly-methyl methacrylate) resist and a deposited silica transfer layer, (figure 5(a)), leads to a much smoother etched surface. Smoothness at this level or better—and nanometre-scale dimensional precision in the pattern transfer—are essential for the future development of both guided-wave photonic crystal and photonic wire components. The use of techniques for further reducing surface roughness [3], after dry-etch pattern-transfer, is also likely to be important.

4. Photonic crystal channel waveguide devices

Once it was recognized and demonstrated that full photonic band-gap (PBG) properties could be obtained—in a 2-space sense and for TE-polarized light—by 'drilling' air-holes into a planar waveguide [4], the logical next step was the creation of channel waveguides by (conceptually) removing lines of photonic crystal elements from the 2D photonic crystal. In the case of hole-based PhCs, the creation of a channel guide is equivalent to filling in one-or-more rows of holes.

[5] Available from Zeon Corporation: http://www.zeon.co.jp/index_e.html

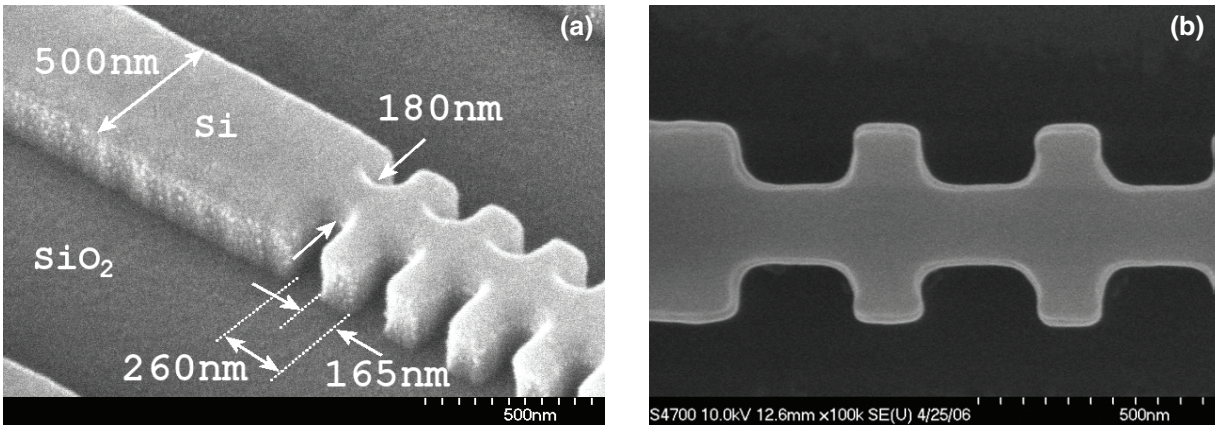

Figure 5. (a) Micrograph of PhW Bragg grating: see [2] and (b) Photonic wire Bragg grating in SOI, after EBL in HSQ resist and transfer into the silicon core via inductively coupled plasma (ICP) etching with silicon tetrachloride.

More generally, the channel waveguide can be considered as being produced by the relative displacement of blocks of photonic crystal by arbitrary amounts, with the further qualification that the modal properties of the defect structures produced must still be determined by electromagnetic computation and/or experimental observation. From the point-of-view of photonic crystal band-structure, the process of creating a channel waveguide is the same as producing a particular form of defect state in the band-gap, and the engineering requirement is to harness this defect state for the conduction of light. But it is a further desirable feature that PhC channel waveguides should be combined to make devices that involve more complex structures. In particular, there is a need for bends, corners and junctions with various geometries and for combinations of these elements to form interferometers, e.g. the Mach–Zehnder interferometer structure that can be made up from two channel-guide *Y*-junctions and four corners or bends. A vital point for efficient transmission of light through the whole PhC channel guide device structure is that a large part of the light injected into it may be reflected back towards the input, even if the output end of the device is perfectly matched to what follows. This point applies even though—in the ideal case—light cannot escape at all from the whole channel structure. The consequence has been that substantial study has been carried out on modifying the properties of the channel guides, more-or-less locally. Detailed exploration of various strategies for optimizing the transmission-bandwidth product of 60° channel waveguide bends in hole-based triangular lattice PhCs has been described in [5], and study based on algorithm-based optimization processes has also been notably successful. The intrinsic questions underlying the use of a computer-based optimization process are whether a sufficiently large parameter space has been selected, and whether a local maximum for the desired property, or combination of properties, is indeed the optimum. A further practical question is the fidelity with which an actual fabricated structure can be made to match the computationally specified one.

The objective of demonstrating an electrically controlled switch or modulator based on photonic crystal channel guides led to the design, fabrication and measurement of a thermo-optically controlled Mach–Zehnder device realized by etching holes deeply into an epitaxial III–V semiconductor planar waveguide [6]. Micrographs of a similar PhC channel-guide Mach–Zehnder device realized in SOI waveguide [7] are shown in figures 6(a) and (b). The thin-film metallic heater electrode in figure 6(a) emphasizes the contrast produced by the holes

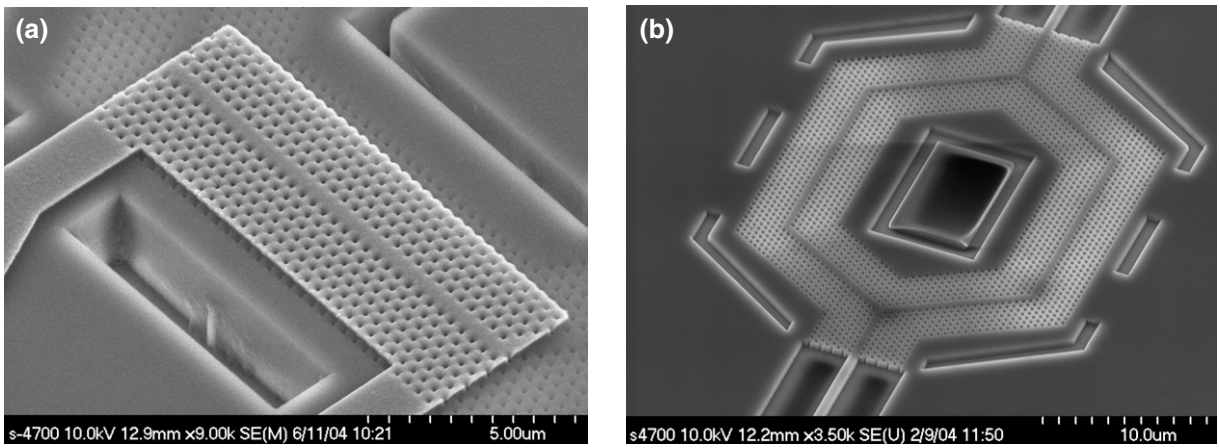

Figure 6. Scanning electron micrograph of (a) part of one arm of PhC channel guide Mach–Zehnder device, showing a nichrome thin-film heater electrode isolated from the planar guide structure by a silica buffer layer and (b) PhC channel guide Mach–Zehnder device, prior to deposition of nichrome thin-film heater electrode.

underneath it, but the penetration of the metallization into the holes is negligible because of the smallness of the hole diametre and the approx. 200 nm of silica deposited prior to the metal deposition.

In our first successful version of a PhC Mach–Zehnder modulator, the structure fabricated was a nominally perfectly symmetric structure with equal arm lengths. The thermo-optic response obtained at an operating wavelength of 1500 nm, close to the centre of the transmission pass-band of the structure, indicated a small amount of asymmetry. But this asymmetry could be attributed principally to the fact that the two arms of the interferometer in the fully realized device were not actually identical, since only one arm was covered, for much of its length, by the metal film heater electrode. The guided optical mode-distribution under this electrode was modified to a significant extent by its presence.

The experimental and simulated transmission spectra for this epitaxial III–V based structure are shown in figure 7. Given the practical factors of imperfect fabrication, the already mentioned presence of some asymmetry, and the limitations of 2D computational simulation of a strictly 3D structure, the agreement is rather good. The presence of some fine ripple structure in the experimental measurements is not surprising, and illustrates an important practical aspect that is characteristic of the strongly confined propagation that occurs in photonic crystal and photonic wire device research. Even quite small partial reflections can lead to strong Fabry–Perot cavity effects. Each point or region where there is a mismatch in the guided light distribution and/or effective index or characteristic propagation impedance can give rise to the partial reflection required for these effects. Reduction of propagation loss, which is itself vitally important for successful implementation of photonic crystal/wire-based integrated optics, also accentuates the need for suppression of all unintentional mismatch. On the other hand, controlled mismatch is exactly what is required for high quality factor (high-Q) resonant cavity effects [8].

We remark that the AlGaAs/GaAs epitaxial planar waveguide used in this device was a weak vertical confinement structure, for which holes penetrating well into the lower cladding region are a requirement for low propagation losses to be possible. Not long after we had successfully

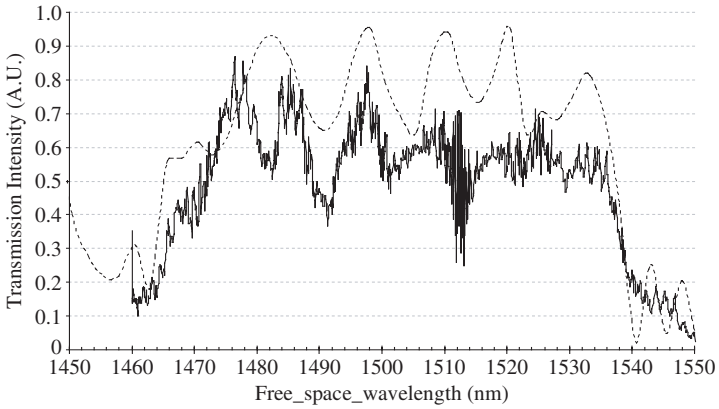

Figure 7. Transmission spectra for AlGaAs/GaAs device: dashed line, simulation; bold line, measured. The measured transmission bandwidth (to a nominal level of −6 dB) was 75 nm, over the range $\lambda = 1465$–1540 nm.

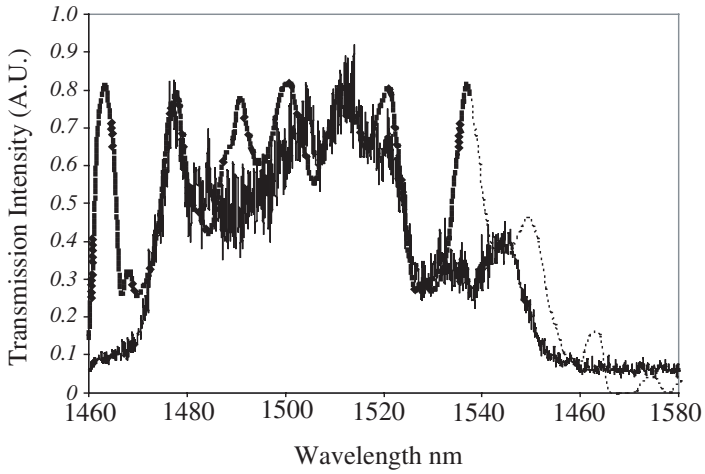

Figure 8. Transmission spectra for Mach–Zehnder PhC device in SOI: dashed line, simulation; bold line, measured. The measured transmission bandwidth is nominally approx. 50 nm, taken over the range $\lambda = 1475$–1525 nm.

demonstrated this basic PhC channel waveguide Mach–Zehnder device in the AlGaAs/GaAs, a closely similar device structure based on SOI waveguide was designed, fabricated and measured. The corresponding computed and measured transmission spectra are shown in figure 8.

The behaviour of the SOI Mach–Zehnder device was found to be similar to that of the AlGaAs/GaAs-based device, despite the much stronger vertical confinement that typically applies for SOI-based planar waveguides. There was also reasonably close agreement between experiment and simulation, although the transmission bandwidths were apparently smaller. One plausible contribution to this inferior performance is that the in-plane index contrast is actually smaller because the effective index for the planar guided mode in the SOI material is significantly smaller than for the AlGaAs/GaAs material.

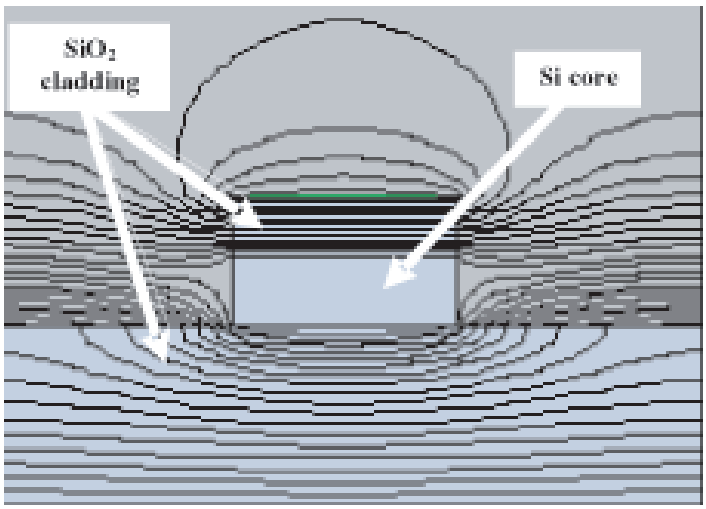

Figure 9. Temperature distribution profile for top heater electrode with silica buffer layer.

Intrinsic drawbacks of our approach to thermo-optic devices are that the thermal energy required for device operation is generated outside the silicon waveguide core, and that the heater electrode is not only isolated optically and electrically from the waveguide core but is also insulated thermally, to a substantial extent, i.e. there is a large thermal resistance to overcome. Figure 9 shows the results of a numerical simulation for the temperature distribution produced in a finite-width silicon waveguide core that is fully surrounded by silica (including a several micrometre thick lower cladding layer), with a heater electrode above the core, and with a finite-thickness (∼200 nm) silica layer between the silicon core and the heat source. The silicon core clearly has its temperature raised by the generation of heat in the electrode above it, but its much greater thermal conductivity means that there is almost no temperature drop across the core. In contrast, the crowded equi-temperature contours in the silica region above the core imply that its temperature is substantially lower than that of the electrode, implying reduced efficiency in the thermal energy delivery process.

Because silicon has a much larger (and positive) value for its refractive index thermo-optic coefficient than silica—and because the net effect of heating silica that is free to expand is the equivalent of a negative change in refractive index—it is desirable to heat the silicon core of the channel guide as directly as possible. Given the small optical propagation distances typically involved a thin layer of a transparent conducting film, such as the indium-tin-oxide (ITO), directly deposited on the silicon core

The Mach–Zehnder devices described above used thermo-optic operation even though, in the case of III–V semiconductor-based devices, the linear (Pockels) electro-optic effect is present and sufficiently strong to make it useful for fully engineered operation at the highest conceivable modulation/switching frequencies. For the case of silicon, the absence of a linear electro-optic effect is a significant drawback that may be overcome using several alternative approaches. The thermo-optic effect is one of these, but possible alternatives can be identified—such as charge carrier injection and confinement modification (depletion-layer width modulation) in junction structures or under the gate of a MOSFET structure. ‘All-optical’ interactions, with ‘light switching light’, may be useful in either III–V semiconductor epitaxial structures or in SOI.

While the centro-symmetric nature of single-crystal silicon dictates that there is no χ_2 behaviour, the non-centro-symmetric nature of the III–V semiconductors implies that parametric processes such as second harmonic generation (SHG) can be harnessed, provided that an appropriate phase-matching structure is used. 'Cascade-χ_2 operation in epitaxial III–V semiconductor waveguides—in which the local sign of the nonlinearity is reversed periodically in conformity with a phase condition corresponding to suppression of SHG—is also of interest because it can provide a stronger χ_3-type interaction than the intrinsic χ_3. In silicon, the potential for exploitation of χ_3 to exploit all-optical functionality is restricted significantly, at communications wavelengths such as $\lambda = 1.55\ \mu$m, by the two-photon absorption process. In contrast, using an all aluminium-GaAs hetero-epitaxial waveguide structure with different aluminium fractions chosen for the core (lower Al-fraction) and cladding regions (higher Al-fraction)—while increasing the minimum Al-fraction, x, in the formula $Al_xGa_{1-x}As$—can completely by-pass the two photon absorption process at the same operating wavelength. For shorter operating wavelengths, the same general principle can be used, possibly with the addition, for example, of phosphorus to the composition to increase the electronic band-gap.

5. Photonic wire Mach–Zehnder devices

Strongly confined optical waveguide propagation can also be obtained in a photonic wire geometry. Furthermore, photonic wire waveguides have been successfully brought together to make compact, low operating-power Mach–Zehnder modulator structures in which the thermo-optic effect has been obtained by direct ohmic heat generation in the silicon waveguide core [9]. Mach–Zehnder interferometers in which much of the structure (i.e. input and output waveguides, *Y*-junctions and bends) was of photonic wire format, while PhC channel waveguides were used in the arms of the interferometer, have been used to demonstrate slow-light propagation via the wavelength-dependence of interferometric variations in the light output [10].

We have designed, fabricated and measured photonic-wire based Mach–Zehnder devices in SOI, choosing to create very compact structures with either a nominally symmetric geometry or the smallest practical levels of geometric asymmetry [11]. The waveguide width, 500 nm, was chosen to give reasonably low propagation losses ($\sim$10 dB cm^{-1}) for the fundamental transverse (even) mode at a wavelength of $\lambda = 1.55\ \mu$m. Plan-view micrographs of symmetric and anti-symmetric interferometers are shown in figures 10(a) and (b) respectively. Corresponding 2D simulations of the power distributions for propagation through the interferometers are shown in figures 11(a) and (b). The almost total leakage out of the waveguide for the exactly anti-phase situation is clearly apparent. For both photonic wire and photonic crystal based waveguide Mach–Zehnder interferometer devices, the anti-phase situation implies leakage of the light into the lower waveguide cladding layer (e.g. for SOI-based structures with air above the guide), and/or into the substrate (e.g. for weakly confined epitaxial III–V semiconductor structures). Fully 3D simulation is required for accurate representation of the situation. In our study, reasonably close agreement was obtained between the experimental transmission spectra and the simulated spectra obtained from 2D finite-difference time-domain (FDTD) computation, with the path length difference between the two arms being the variable parameter.

In order to obtain a close approximation to 100% transmission through the interferometer, detailed simulation and design were carried out on both the bend and *Y*-junction geometries. The sharp wedge-opening for the 60° *Y*-junction shown in the micrograph of figure 12(a) was found

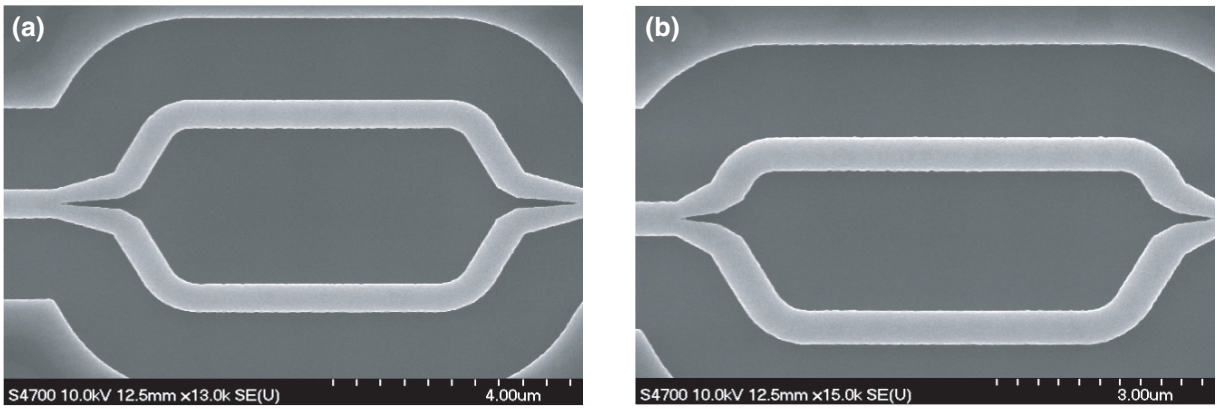

Figure 10. (a) Ultra-compact photonic-wire based symmetric Mach–Zehnder structure and (b) asymmetric photonic-wire Mach–Zehnder structure.

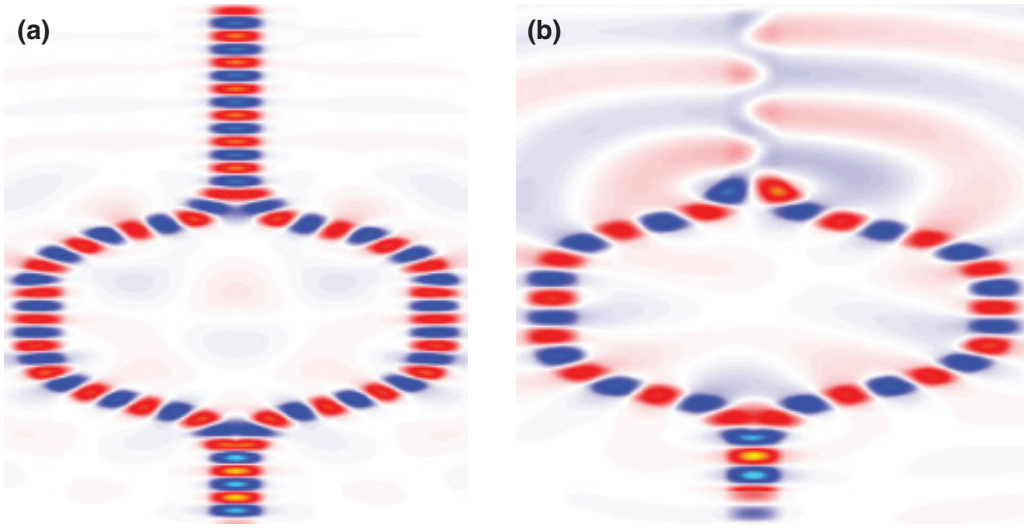

Figure 11. Sign-dependent field distribution for (a) symmetric and (b) asymmetric photonic wire Mach–Zehnder structure.

to be effective in this respect, and the exact shape of the bend shown in figure 12(b) likewise. Only EBL has the intrinsic resolution required to make the wedge-opening feature of figure 12(a) a feasible proposition. The wall roughness clearly visible in these two micrographs results primarily from the two-stage pattern transfer process used, with a combination of ZEP organic resist and a deposited silica intermediate layer. The degree of roughness exhibited would be considered as unacceptably large in a fully engineered integrated optical sub-system.

The absolute path lengths through the interferometer structure were small, so that the resulting transmission spectra were fairly flat over the measured wavelength range, and even the predominant Fabry-Perot ripple was associate with a short enough cavity length that it was a fairly coarse and small feature superimposed on the Mach–Zehnder response. To obtain the best agreement between experiment and simulation, it was found that the structure simulated had to have built-in modal filtering action, obtained by narrowing the wire waveguides equally in identical parts of each arm of the interferometer. We believe that this modification in the 2D

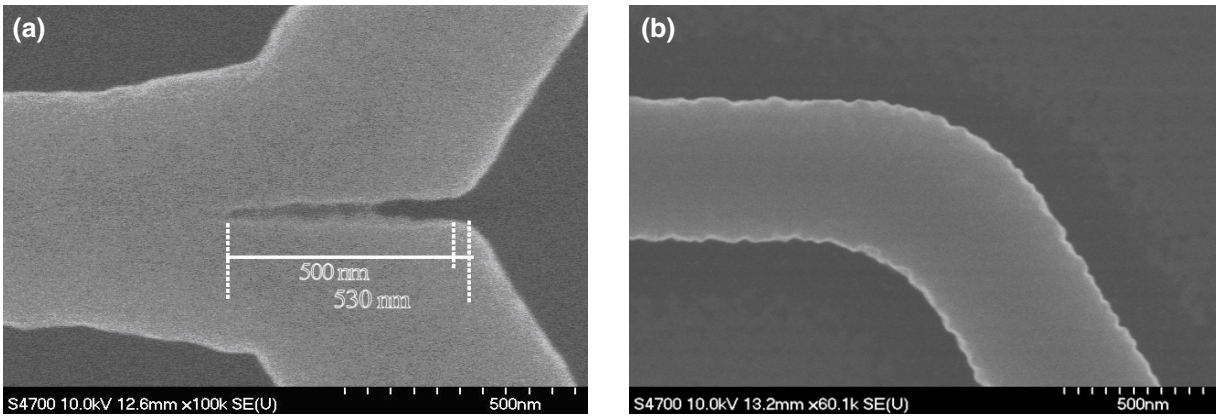

Figure 12. Plan-view micrograph of part of fabricated photonic wire waveguide (a) *Y*-junction and (b) 60° bend.

numerical simulation has much the same effect on leakage of light out of the structure as would appear in a 3D simulation that modelled the effects of leakage into the lower cladding. Successful demonstration of the strongly wavelength-dependent interference effects obtainable with highly asymmetric Mach–Zehnder interferometers is described in [12].

6. Finite area photonic crystal elements

Limited areas of planar waveguide photonic crystal can provide a variety of useful functions, including lenses, input/output couplers, beam-splitters, partial or near-total mirrors and power dividers [13]–[15]. Valuable demonstrations have been made of the role of the frequency dependent spatial dispersion behaviour, in particular, of square-lattice 2D photonic crystal regions in producing auto-collimation behaviour [16].

Such photonic crystal elements may usefully be embedded in waveguide structures that have widths that are several (e.g. ten) lattice constants across the main propagation axis. An example of a device structure that has considerable potential for practical applications such as demultiplexing in wavelength division multiplexing (WDM) communication systems is the waveguide Fabry-Perot cavity formed by a several micrometre long spacer section between two mirrors [17]. A micrograph of a basic device structure that has been fabricated and tested is shown in figure 13(a). The full thermo-optic device, with a 120 nm thick, approximately 1 kΩ, nichrome heater electrode superimposed on a approximately 300 nm thick silica buffer layer is shown in figure 13(b).

Experimental results obtained with the fabricated structure are shown in figures 14(a) and (b). Because of the specific choice of the length of the cavity spacer section at a nominal value of 8 μm, one of the several longitudinal (axial) modes of the cavity could be selected to match with an operating wavelength of approx. 1527 nm.

Experimentally demonstrated Q-factor values of approaching 2000—and the plausibility of obtaining values a factor of two larger—imply that a viable scanning channel-drop filter device could be produced with modest refinements in the design and fabrication of the device. Changing the temperature of the silicon core by approximately 300 °C should be sufficient to scan across the whole of the available free spectral range of 37 nm.

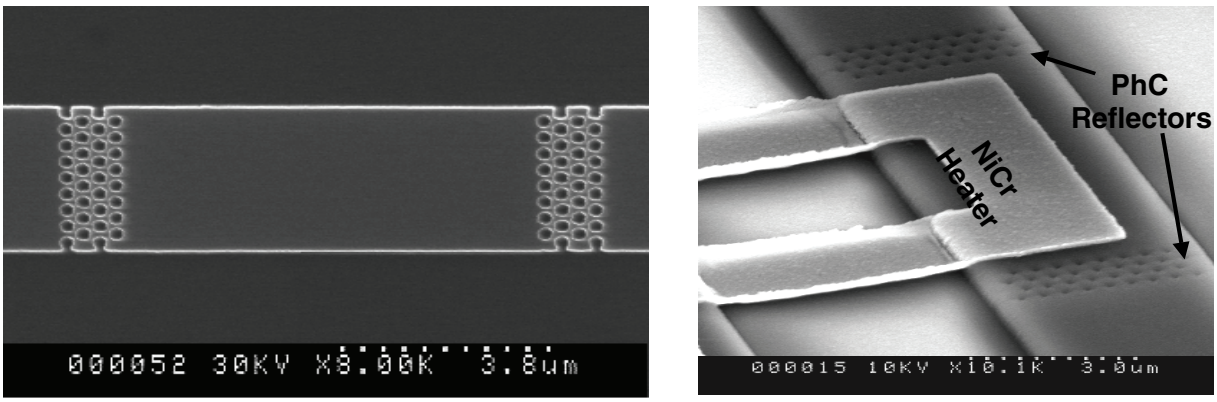

Figure 13. (a) Long Fabry-Perot cavity with two photonic crystal mirrors and (b) thermo-optically operated PhC mirror Fabry-Perot cavity device.

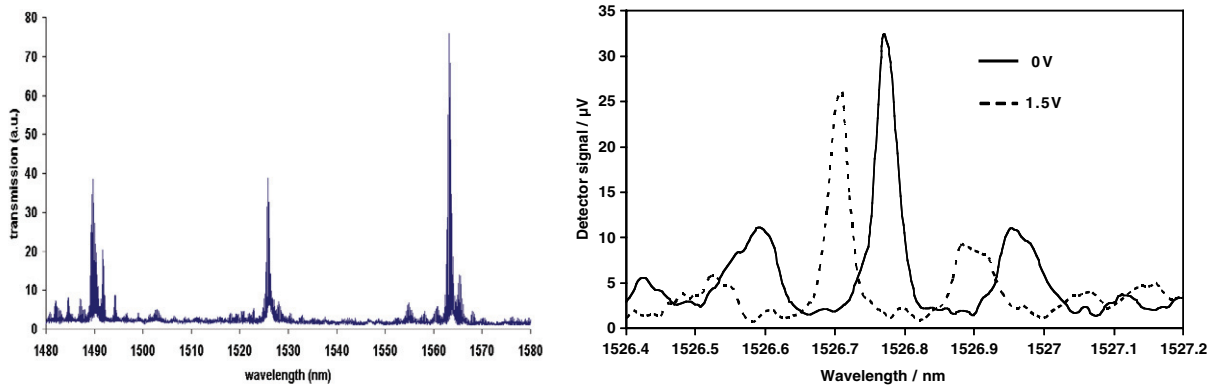

Figure 14. (a) Transmission characteristics of the 8 μm long PhC Fabry-Perot filter and (b) expanded view of transmission versus wavelength around the selected main-peak, without (bold line) and with (dashed line) application of thermo-optic effect.

But somewhat surprising features were actually observed in the transmission spectrum when viewed at high resolution. Instead of the relatively large red-shift expected because of the positive temperature coefficient of silicon, it was possible to identify a small (0.06 nm) blue-shift. The observation of the spectral shift was facilitated by the presence of the additional finely featured Fabry-Perot fringe-pattern that resulted from the weak (ca 30%) reflections at the sample ends. The fact that a blue-shift is observed indicates that a combination of factors has reduced the impact of heating of the silicon core. A full analysis of the situation would require modelling of heat-flow and the resulting temperature distribution, optical mode-distribution and stress/strain-optical effects in the whole silicon-core/silica-cladding structure.

Two positive conclusions arise from these somewhat surprising results. (i) It may well be possible to construct a Fabry-Perot filter device, similar to the one already demonstrated, in which the operation could be completely or almost completely temperature-independent. (Such temperature-independent operation has already been demonstrated in silicon-silica Bragg-mirror stacks, which may be regarded as being a form of 1D photonic crystal [18].) Alongside this temperature-independent operation (in terms of changes in the general ambient surrounding

the device), applying a localized temperature increase by direct heating of the waveguide core could still give temperature-controlled thermo-optic tuning of the device. Detailed simulation (eventually involving 3D computation) would still be required to hit a given target operating wavelength reliably to within ± 1 nm. Corresponding precision would be required in the fabrication. Even if nearly perfect athermal operation were achievable, tuning to a standard reference wavelength might still be required. (ii) It is possible to construct a multiple (e.g. double or triple) cavity combination, with different spacing between adjacent 2D PhC mirrors, that has a substantially enhanced Q-factor, e.g. values as large as the approximately 20 000 implied by the results of figure 14(b). Clearly the mirror-spacing must be comparable with the 8 μm length of the demonstrated nominally single-cavity device if the free spectral range value is also to remain as large as 37 nm.

7. Concluding remarks

In this paper, we have explored some of the device possibilities offered by applying photonic crystal and/or photonic wire concepts on a silicon-based planar waveguide basis. In particular, consideration has also been given to the prevailing situation where epitaxial III–V semiconductors continue to form the normal basis for the vitally important functions of light emission and light detection. The results of research on various single and coupled micro-cavity structures have not been presented here, but appear in the published literature [19, 20]. A short review feature has also appeared recently [21].

Our view, despite exciting developments such as the silicon Raman laser, is that silicon integrated optics still automatically implies a hybrid approach to the task of device integration. But functions such as electrically- or optically-controlled switching and modulation, tunable filtering and variable beam-splitting, actively controlled focussing and collimation all appear to be practical. Epitaxial III–V semiconductors arguably are capable of providing superior performance, e.g. for all-optical device operation at high modulation rates [22], and acceptance of their greater intrinsic technological complexity may prove to be a price that is worth paying. Although achieving fully monolithic integration remains more probable using III–V semiconductors than using silicon, the hybrid approach may still be inescapable in either case.

The application, in future integrated optoelectronics, of photonic crystal and photonic wire concepts will be essential in the quest for compactness, low-voltage/low-power operation and superior performance more generally.

Acknowledgments

Our study on photonic crystal and photonic wire devices has been supported by the EPSRC (UK) in the Ultrafast Photonics Collaboration, by the European Community in the PICCO project and by British Aerospace.

References

[1] Jin C, McLachlan M A, McComb D W, De La Rue R M and Johnson N P 2005 Template-assisted growth of nominally cubic (100)-oriented three-dimensional crack-free photonic crystals, *NanoLetters* **5** 2646–50

[2] Gnan M, Bellanca G, Chong H M H, Bassi P and De La Rue R M 2006 Modelling of photonic wire Bragg gratings *Opt. Quantum Electron.* **38** 133–14

[3] Sparacin D K, Spector S J and Kimerling L C 2005 Silicon waveguide sidewall smoothing by wet chemical oxidation *IEEE J. Lightwave Technol.* **23** 2455–61
[4] Krauss T F, De La Rue R M and Brand S 1996 Two-dimensional photonic bandgap structures at near infrared wavelength *Nature* **383** 699–702
[5] Ntakis I, Pottier P and De La Rue R M 2004 Optimization of transmission properties of two-dimensional photonic crystal channel waveguide bends through local lattice deformation *J. Appl. Phys.* **96** 12–18
[6] Camargo E A, Chong H M H and De La Rue R M 2004 2D Photonic crystal thermo-optic switch based on AlGaAs/GaAs epitaxial structure *Opt. Express* **12** 588–92
[7] Camargo E A, Chong H M H and De La Rue R M 2006 Highly compact asymmetric Mach–Zehnder device based on channel guides in two-dimensional photonic crystal *Appl. Opt.* **45** 6507–10
[8] Song B S, Noda S, Asano T and Akahane Y 2005 Ultra-high-Q photonic double-heterostructure nanocavity *Nature Mater.* **4** 207–10
[9] Geis M W, Spector S J, Williamson R C and Lyszczarz T M 2004 Submicrosecond submilliwatt silicon-on-insulator thermooptic switch *IEEE Photon. Technol. Lett.* **16** 2514–16
[10] Vlasov Y A, O'Boyle M, Hamann H F and McNab S J 2005 Active control of slow light on a chip with photonic crystal waveguides *Nature* **438** 65–9
[11] Zhang H, Gnan M, Johnson N P and De La Rue R M 2006 Ultra-small Mach–Zehnder interferometer devices in thin silicon-on-insulator, integrated photonics research and applications topical meeting, Uncasville, CT, 24–26 April 2006, paper ItuB3
[12] Ohno F, Fukazawa T and Baba T 2005 Mach–Zehnder interferometers composed of μ-bends and μ-branches in a Si photonic wire waveguide *Japan. J. Appl. Phys.* **44** 5322–3
[13] Pottier P, Mastroiacovo S and De La Rue R M 2006 Power and polarization beam-splitters, mirrors, and integrated interferometers based on air-hole photonic crystals and lateral large index-contrast waveguides *Opt. Express* **14** 5617–33
[14] Wu L J, Mazilu M, Gallet J F, Krauss T F, Jugessur A S and De La Rue R M 2004 Planar photonic crystal polarization splitter *Opt. Lett.* **29** 1620–2
[15] Taillaert D, Chong H, Borel P I, Frandsen L H, De La Rue R M and Baets R 2003 A compact two-dimensional grating coupler used as a polarization splitter *IEEE Photon. Technol. Lett.* **15** 1249–51
[16] Shi S, Sharkawy A, Chen C, Pustai D M and Prather D W 2004 Dispersion-based beam splitter in photonic crystals *Opt. Lett.* **29** 617–9
[17] Ciminelli C, Chong H M H, Peluso F, De La Rue R M and Armenise M N 2004 High Q guided-wave photonic crystal extended microcavity, ECOC 2004, Stockholm (5–9 Sept. 2004), Post-Deadline papers Th4.2.6 pp 26–7
[18] Weiss S M *et al* 2004 Temperature stability for photonic crystal devices (Optics in 2004 special issue) *Opt. Photon. News* **15** (12) December 2004
[19] Chong H M H and De La Rue R M 2004 Tuning of photonic crystal waveguide microcavity by thermo-optic effect *IEEE Photon. Technol. Lett.* **16** 1528–30
[20] Jin C, Johnson N P, Chong H M H, Jugessur A S, Day S, Gallagher D and De La Rue R M 2005 Transmission of photonic crystal coupled-resonator waveguide (PhCCRW) structure enhanced via mode matching *Opt. Express* **13** 2295–302
[21] De La Rue R M 2006 Photonic crystal components: harnessing the power of the photon *Optics and Photonics News*, July/August 2006, pp 30–5
[22] Nakamura H *et al* 2004 Ultra-fast photonic crystal/quantum dot all-optical switch for future photonic networks *Opt. Express.* **12** 6606–14